

Laser-Cantilever-Anemometer

A new high resolution sensor for air and liquid flows

Stephan Barth,* Holger Koch, Achim Kittel, and Joachim Peinke
Carl von Ossietzky University of Oldenburg, D-26111 Oldenburg, Germany

Jörg Burgold and Helmut Wurmus
Center for Micro- and Nanotechnologies, D-98684 Ilmenau, Germany

(Dated: May 17, 2005)

In this paper we present a technical description of a new type of anemometer for gas and especially liquid flows with high temporal and spatial resolution. The principle of the measurement is based on the atomic force microscope technique where micro-structured cantilevers are used to detect extreme small forces. We demonstrate the working principle and the design of the sensor, as well as calibration measurements and initial measurements of turbulent flows, which were performed in air and water flows.

PACS numbers: 47.27.JV, 47.80+v

I. INTRODUCTION

In fluid mechanics and especially in turbulence research there is a large interest in high resolution velocity measurement techniques. Aside from well established methods like laser doppler anemometry where the flow velocity is detected contactless by laser beam, or hot-wire anemometry with very high spatial and temporal, resolution there remains a demand for the development of new techniques. Some examples of recent developments are methods that allow the measurement of the velocity in Lagrangian coordinates, i.e. the measurement of the velocity of a fluid particle and its trajectory. Detectors from high energy physics¹ or alternatively arrays of fast ultrasonic actuators and detectors² have been used. Further examples of recent developments are techniques that use the nuclear magnetic resonance (NMR) to measure, for instance, the flow field in a falling drop,³ the RELIEF-method where molecules are marked by a laser light-section and the deformation of the section provides some information on the flow^{4,5} or holographic particle imaging techniques to map the three-dimensional velocity distribution of complex nonstationary flows.⁶

Hot-wire anemometers have been used for several decades as suitable velocity detectors and have been until now standard sensors for high resolution velocity measurements. This holds in particular for turbulence experiments where small scale effects are investigated. The sensors are heated by a current while being cooled simultaneously by the passing fluid. Operated in a constant temperature mode the required current yields the information of the fluid velocity. The small dimensions of such sensors cause a very small heat capacity which allows for a dynamical response up to some tens of kHz.^{7,8} Due to

the high resolution combined with the technically mature development status, founded by the long optimization-time, we compare the results we received with our sensor to those received with the hot-wire anemometer. Despite the success of hot-wire anemometry this technique has reached its limits. Wires with a diameter smaller than $1 \mu\text{m}$ aren't mechanically stable enough to be used in flow experiments. The required aspect ratio^{7,8} (length to diameter) of 100:1 fix their length to a lower limit of $100 \mu\text{m}$.⁹ Another limitation is imposed on the hot-wire anemometry in water experiments. Here the overheat ratio of the wires, the temperature difference to the flowing fluid, have to be much smaller than in air, which confines their sensitivity. In addition for conductive flows the wires need to be electrically isolated which increases the thermal mass of the sensor and makes the system even less sensitive. Due to its design a hot-wire is always a non-shielded part of the amplifier circuit of a hot-wire anemometer thus acting as an antenna. Thereby hot-wire anemometers are more susceptible to high frequency electro magnetic interference.

These limiting factors of the hot-wire anemometry are the starting point for the development of a new type of anemometer, the Laser-Cantilever-Anemometer (LCA) which is based on the atomic force microscope technique. At the present time we are able to show the working principle and to present measurements with a prototype which already reaches the resolution of hot-wire anemometry.

It is an open problem to characterize a sensor's dynamics in an environment with highly fluctuating properties. In^{10,11} a micronic-size cryogenic thermometer for fast turbulence measurements was presented, from which we got the idea to show the dynamic response features of our sensor by the reproduction of characteristic features of turbulence.

The paper is structured as follows, first we discuss in section 2 the working principle of the LCA, next in section 3 the details of the construction of the prototype are presented. In section 4 dynamics of electronics that

*Also at ForWind - Center for Wind Energy Research, Marie-Curie-Str. 1, D-26129 Oldenburg, Germany; Electronic address: stephan.barth@uni-oldenburg.de; URL: <http://www.forwind.de>

is used is discussed and in sections 5 and 6 the calibration as well as initial measurements are presented.

II. WORKING PRINCIPLE

Based on the atomic force microscope (AFM) technique,¹² micro structured cantilevers with a typical length of $160 \mu\text{m}$, a width of $30 \mu\text{m}$ and a thickness of $1\text{-}3 \mu\text{m}$, which are normally used to resolve atomic distances and forces, are used as sensing elements. To perform local velocity measurements in a fluid, we detect the deflection s of the cantilever due to the drag force.

In contrast to the usual application in atomic force microscopes, loads along the whole surface instead of just loads on a well defined point act on the cantilever. The deflection of the tip of the cantilever is therefore described by¹³

$$s = \frac{l^3}{8} \frac{F}{E \times I_a}, \quad (1)$$

with the elasticity modulus E , the force F and the second moment of area for a rectangular cross-section $I_a = \frac{1}{12}wh^3$ for a plate with dimensions $l \times w \times h$ (length, width, height). In this case the force acting on the cantilever is caused by the component of the flow velocity v which is normal to the cantilever surface.

$$F = c_d \times \frac{1}{2} \times \rho \times v^2 \times l \times w, \quad (2)$$

with c_d as drag coefficient and ρ as density of the fluid. According to Eq.1 and Eq.2 the deflection s is given by

$$s = \frac{3 \times c_d \times \rho \times v^2 \times l^4}{4 \times E \times h^3}. \quad (3)$$

Note that the deflection is independent of the width of the cantilever, and v is the value of the fluid velocity averaged over the cantilever.

Due to the small dimensions and the very sharp edges of the cantilever we take the drag coefficient to be independent of the Reynolds number, which will be verified by calibrations.

To detect the deflection of the cantilever we focus a laser beam on the tip of the cantilever and measure the position of the reflex spot with a position sensitive detector (psd), see figure 1.

The linear psd of length L_X which we use to get the position of the reflected light yields two electric currents I_{X1} and I_{X2} at the ends of the photosensitive surface (figure 2)

$$I_{X1} = I_0 \frac{L_X - X_B}{L_X}, \quad I_{X2} = I_0 \frac{X_B}{L_X}, \quad (4)$$

with I_0 as the light intensity.¹⁴ The following quantity

$$\mathcal{U} = \frac{I_{X1} - I_{X2}}{I_{X1} + I_{X2}} = \frac{I_0 \left(\frac{L_X - X_B}{L_X} - \frac{X_B}{L_X} \right)}{I_0 \left(\frac{L_X - X_B}{L_X} + \frac{X_B}{L_X} \right)} = 1 - \frac{2}{L_X} X_B \quad (5)$$

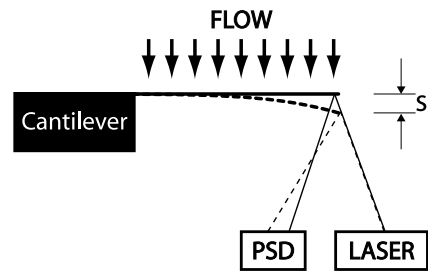


FIG. 1: Cantilever deflection s with flow (dashed lines) and without flow (solid lines). Detected by a laser and position sensitive detector (PSD).

is a linear function of the reflex position X_B and is independent of the intensity I_0 . This means any changes in the light intensity which are acting on the whole PSD element, e.g. the ambient light or variances in the laser intensity, will not affect the position measurement.

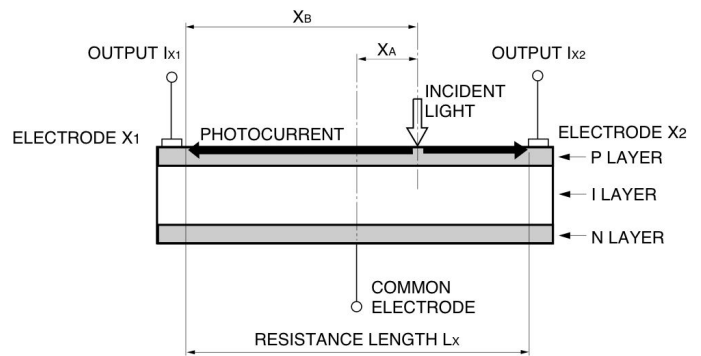


FIG. 2: Schematic of the psd element with the used nomenclature. P stands for positive doped, I for isolator and N for negative doped.

III. DESIGN

The design of the LCA is shown in figure 3. At the tip of the device (left lower end of the figure 3) a small arm is attached, at the end of which the cantilever is glued. The waterproof enclosure contains the psd element with its amplifier electronics, the laser with optical components and step motors to adjust the laser beam orientation. In the following we will describe each parts in detail.

To measure the velocity to a high degree of accuracy the chip which is the base of the cantilever is designed as shown in figure 4, micrograph. The cantilever is held in position by two $20 \mu\text{m}$ wide bridges. Etching a window into the chip gives the advantage that the fluid can pass the vicinity of the cantilever unhindered. Thus close to the cantilever the disturbance of the flow is kept small.

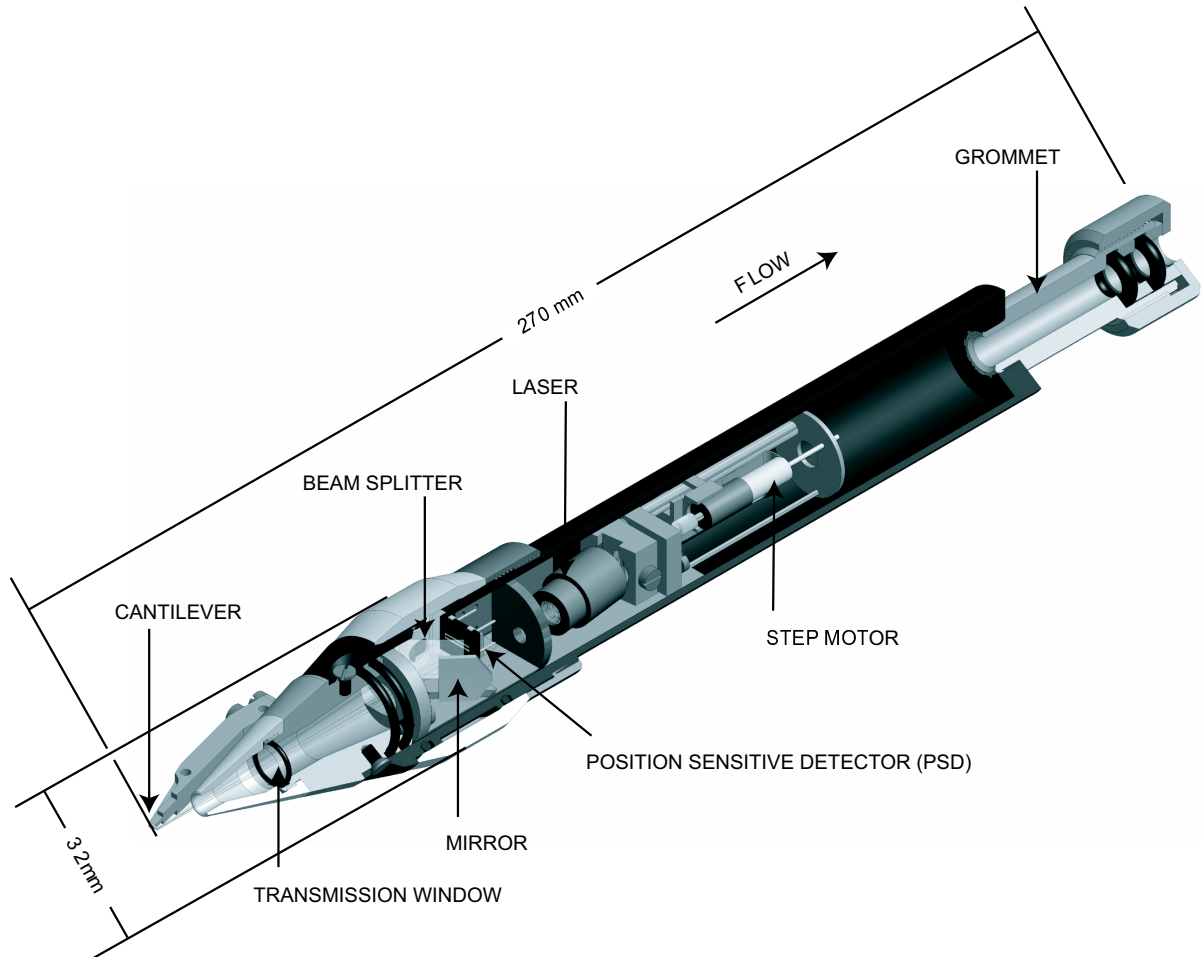


FIG. 3: 3D illustration of the Laser-Cantilever-Anemometer with the labeled components.

To produce these kind of cantilever chips, a $300\ \mu\text{m}$ thick silicon wafer, with (100) crystal orientation, is thermally oxidized at 1323 K and then micro-structured by several wet-etching and plasma-etching processes. The last process step is to cover the transparent quartz-cantilever by evaporating chromium to get a high reflectivity.

The arm on which the cantilever chip (see figure 4 right part) is glued has a front surface not bigger than the cantilever chip itself, actually $1.8\ \text{mm} \times 1\ \text{mm}$, see figure 4, left picture. The arm is tapered in three steps to reduce the dimensions as much as possible but still keep the mechanical stability.

To achieve the small diameter of the entire LCA-instrument (currently 25 mm) the laser and the psd element are not arranged side by side but in a row. This is done by tilting the laser unit and using a mirror and a 50 % beam splitter as shown in figure 5.

At the front the LCA is closed by a transmission window (see figure 3) made out of BK7 glass with an ARB2-IR anti reflex layer to avoid the direct reflection from the outgoing laser light back to the sensor. The ARB2-IR is a broadband anti-reflex layer supported by Linos

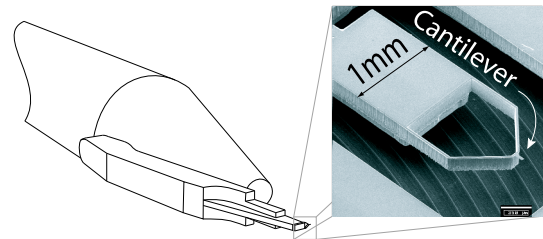


FIG. 4: Top view of the LCA and the arm on tip of which the cantilever is glued. In the micrograph a cantilever chip is shown. The cantilever is the tiny rectangle at the very end of the windowframe.

photonics.

The laser unit consists of a RLD-65MC 7 mW laser diode (655 nm) from ROHM and a full plastic a-spherical collimator lens CAW100 from PHILIPS with a focal length of 9.85 mm at 785 nm wavelength.

To adjust the laser orientation two small 0615C step motors with 06/1 planetary gears from FAULHABER (together 6 mm diameter, 25 mm length) are built in,

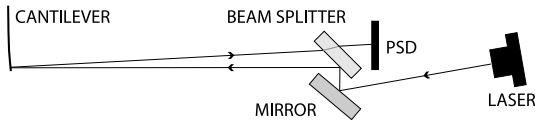


FIG. 5: Illustration of the path of light within the Laser-Cantilever-Anemometer.

making it possible to tilt the laser independently in the vertical and horizontal directions. The spatial resolution of the positioning on the cantilever is about $4 \mu\text{m}$. This positioning is required especially for the use of the LCA in liquids. Inserted into the liquid, it is still possible to adjust the optical path properly, to optimize the sensitivity of the sensor.

As shown in figure 5 the laser light, reflected by the cantilever goes through the beam splitter on a psd element SSO-EL6-6 with an photosensitive length of $L_X = 6 \text{ mm}$. The two currents described in Eq. 4 are amplified by a trans-impedance amplifier circuit, figure 6. Those

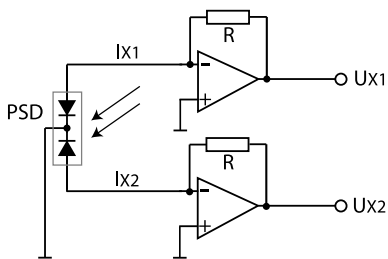


FIG. 6: Trans-impedance amplifier circuit used in the LCA.

kind of circuits yield an output voltage (U_{X1} , U_{X2}) that is linear to the input current (I_{X1} , I_{X2}). In the following we only use the voltage signals. In the LCA we use a TL072CP integrated circuit which includes two low noise operational amplifiers. To avoid disturbances from interfering electronic signals the metallic enclosure and the system have a common ground.

IV. TESTING OF THE ELECTRONICS

Beside the high spatial resolution, given by the small dimensions of the cantilever, the LCA should also yield the velocity information with a high temporal resolution. To check this we performed tests with the psd and the amplifier unit and we used a LED powered by a square wave from a signal generator and observed the response time of the LCA output signal. Because a response time of the LED less than 500 ns is easily achieved¹⁵ we directly compare the LCA output signal with the square wave of the signal generator, see figure 7. As one can see the electronics reached the $10/90$ value within $10 \mu\text{s}$. Thus the present LCA-electronics are fast enough to measure velocity fluctuations up to 100 kHz .

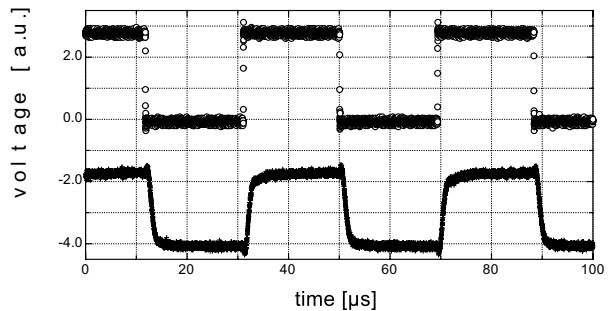


FIG. 7: Response of the electronics (lower trace) on LED powered by a signal generator (upper trace). Both curves are shifted vertically for clarity of presentation.

V. CALIBRATION

Like the hot-wire the LCA yields no absolute velocity signals and therefore has to be calibrated. In contrast to King's Law for the hot-wire, where the signal $U[V]$ is a function of the velocity⁷ $v[m/s]$, $U \propto v^{0.25}$, we expect the LCA to follow a v^2 dependence as described in Eq. 3. This means that the nonlinearity is strongly reduced, which is important for the resolution and the signal to noise ratio of the system. In figure 8 the two recorded output signals (signal-to-noise ratio 40.12 dB) (see figure 6) are shown. The calibration points were obtained in

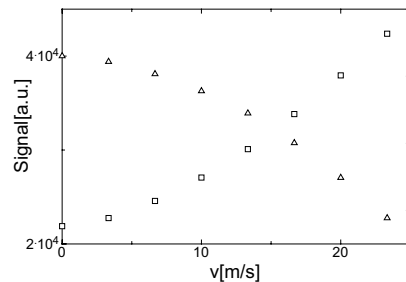


FIG. 8: Calibration measurement of the LCA. Triangles represent the recorded signal U_{X1} and squares U_{X2} .

a laminar wind tunnel from digitalized signals U_{X1} and U_{X2} . The best calibration fit is given by $v = -4.46 + 35.4\sqrt{U + 0.31}$, according to Eq. 5, see figure 9.

VI. INITIAL RESULTS AND DYNAMICAL CHARACTERIZATIONS

So far we have presented the calibration for laminar flow conditions. Our aim is to develop a new anemometer for turbulent flows. For such highly fluctuating flows it is an open problem to characterize anemometers. Thus we verify our results by well known features of local isotropic turbulence with respect to small scales. In this section

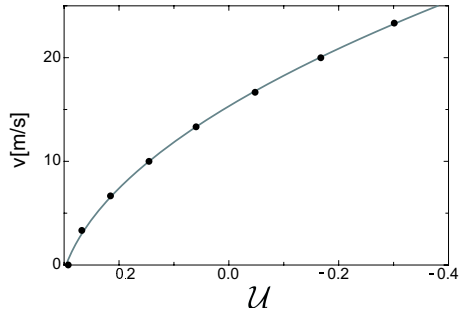


FIG. 9: Calibration curve according to Eq. 3 and 5 (filled symbols: measurement, line: fit with $v = -4.46 + 35.4\sqrt{U + 0.31}$).

we present initial measurements and the mentioned dynamical characterizations. We compare the results with a hot-wire anemometer StreamLine Research CTA system from Dantec Dynamics and a 55P01 hot-wire probe.

The following results are all based on a free jet experiment with air into air. The diameter of the nozzle outlet is $d = 8$ mm where the velocity is $v = 34$ ms⁻¹. The resulting Reynolds number is $Re \approx 17500$.¹⁶ Turbulence measurements were performed at a distance of $37.5 d$ downstream in the center of the free jet with a mean flow at the position of $\bar{v} = 12$ ms⁻¹. The measured raw output signals were converted into velocities according to $v = -4.46 + 35.4(U + 0.31)^{0.5}$ for the LCA and $v = -0.14 + 4.91(U - 0.75)^4$ for the hot-wire after King's Law,⁷ U is the calculated signal according to Eq. 5, U is the output signal of the hot-wire anemometer. Regarding the power spectra of the air free jet (figure 10) one can see that the LCA and the hot-wire measurements coincide within the inertial range of $-5/3$ (Kolmogorov law) and down to the dissipation range ($f < 10$ kHz).

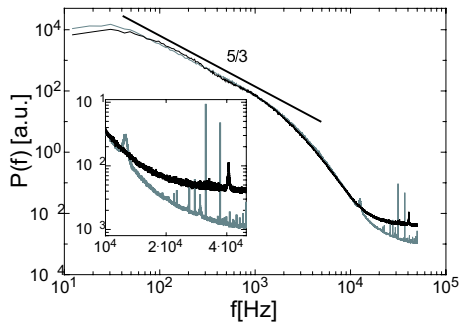


FIG. 10: Power spectra of the free jet experiment, cantilever: black line, hot-wire: gray line.

Note the interfering signals of the hot-wire signal at high frequencies (larger than 10 kHz) (see enlargement in figure 10). These perturbations do not appear in the cantilever signal because of the shielded enclosure.

For the next step in comparing the LCA and hot-wire measurements we look at the multiscaling properties of the turbulent signals. The multiscaling properties are

of actual interest in turbulence research and represent a more detailed analysis, c.f.^{17,18}. Thus we calculated the probability distribution functions (pdfs) $p(\delta v(r))$ for different length scales r of velocity increments¹⁹

$$\delta v(r) := v(x) - v(x+r), \quad (6)$$

and their higher order moments (structure functions)

$$\langle \delta v(r)^n \rangle = \int_{-\infty}^{\infty} p(\delta v(r)) \times (\delta v(r))^n d\delta v(r). \quad (7)$$

The velocity increments are obtained from velocity measurements in time by Taylor's hypothesis of frozen turbulence c.f.²⁰ $x = \bar{v} \times t$; \bar{v} is the mean velocity.

As one can see in figure 11 the pdfs coincide quite well.²¹ The deviations of the pdfs for small scales and positive velocity increments are up to now not explained, but belong to the dissipative and measurement noise range (> 5 kHz) of the power spectra (figure. 10).

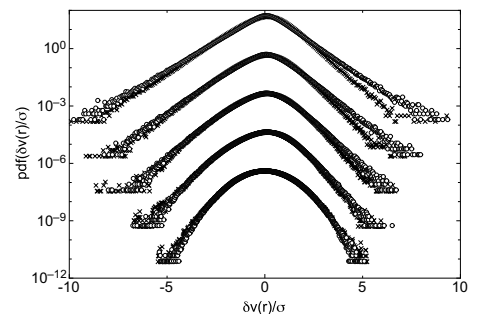


FIG. 11: Velocity increment pdfs of the hot-wire (crosses) and the LCA (circles) for the length scales 1 mm, 2 mm, 4.7 mm, 13.3 mm and 106.2 mm (from top to bottom). The pdfs are shifted away from each other in y-direction for clarity of presentation.

A further characterization is done by using Benzi's method of extended self-similarity (ESS),²² $\langle \delta v(r)^n \rangle \propto \langle |\delta v(r)^3| \rangle^{\xi_n}$. In figure 12 the scaling exponent ξ_n of structure functions of degree n is plotted. The LCA yields the same results as the hot-wire even for $n > 8$ where the estimation of the scaling exponent normally becomes more and more uncertain, see for example.¹⁷

In a simple water into water free jet setup we compared the LCA with a commercial available high resolution Dantec 55R01 hotfilm probe, which has a frequency limit of 30 kHz according to the manufacturer. Again a nozzle ($d = 8$ mm) was used. The velocity at the nozzle exit is $v_{nozzle} = 8$ ms⁻¹. The resulting Reynolds number is $Re \approx 40000$. Turbulence measurements were performed at a distance of $50 d$ downstream in the center of the free jet. While increasing the flow rate and thus the Reynolds number, the $-5/3$ inertial range is expanding towards higher frequencies as expected for turbulent flows, see figure 13. For the highest flow rate (equivalent to 8 ms⁻¹ at the nozzle) the power spectrum is compared

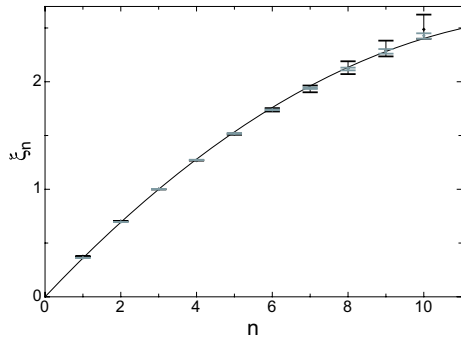


FIG. 12: Scaling exponent ξ_n estimated by extended-self similarity from the LCA dataset (black) and the hot-wire dataset (grey). The solid line represents a fit with $\xi_n = \frac{n}{3} - \frac{\mu}{18}n(n-3)$, $\mu = 0.24$, which is well in the range of $\mu = 0.26 \pm 0.04$ according to.²³ Error bars for ξ_n were obtained after a method described by Peinke.²⁴

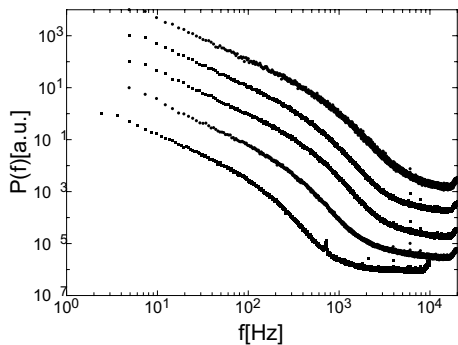


FIG. 13: Power spectra of the water free jet measurement for different flow rates, increasing from bottom to top are shown. The spectra are shifted away from each other in y-direction for clarity of presentation.

to the spectrum measured with the hotfilm, see figure 14. As the power spectrum of the LCA measurement shows characteristics of a typical turbulent flow, the power spectrum of the hotfilm measurement shows no significant $-5/3$ scaling. We interpret that as a hint that the hotfilm was not able to acquire all properties of the turbulent signal. Thus while one of the best commercial available hot wire anemometers already has difficulties in this simple but strongly fluctuating flow, we obtain promising results for our new technique.

The next steps will be further investigations in water experiments and improvements in the technique. Instead of using a laser to measure the deflection we plan to integrate strain gauges into the cantilever thus the size of the LCA instrument can be reduced.

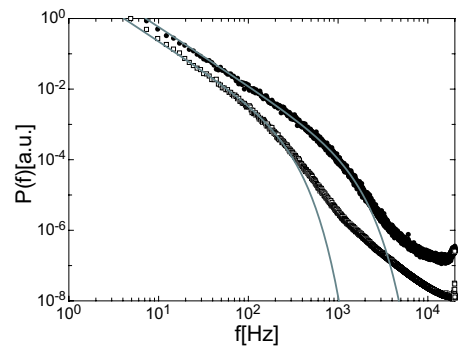


FIG. 14: Power spectrum of the water free jet measurement with the LCA (filled circles) and the hotfilm anemometer (open squares) and fits (grey curves) after Pao^{25,26} are shown.

VII. ACKNOWLEDGEMENTS

The authors acknowledge helpful discussion with Stephan Lück, Marco Munzel, the Interdisciplinary Turbulence Initiative, especially Ronald du Puits and Christian Resagk as well as the financial support by the DFG (grant no.: Pe478/7).

BIBLIOGRAPHY

- ¹G. A. Voth, A. La Porta, A. Crawford, C. Ward, E. Bodenschatz and J. Alexander, *Rev. Sci. Instrum.* **12**, 4348 (2001).
- ²N. Mordant, O. Michel, P. Metz, J.-F. Pinton, *Phys. Rev. Lett.* **87**, 214501 (2001).
- ³S. Han, S. Stapf and B. Blümich, *Phys. Rev. Lett.* **87**, 144501 (2001).
- ⁴T. Elenbaas, W. Van de Water, N. Dam and J.J. ter Meulen, *Advances in Turbulence IX*, (CIMNE, Barcelona, 2002), p. 137.
- ⁵A. Noullez, G. Wallace, W. Lempert, R.B. Miles and U. Frisch, *Jour. Fluid Mech.* **339**, 287 (1997).
- ⁶S. F. Herrmann and K. D. Hinsch, *Meas. Sci. Technol.* **15**, 613 (2004).
- ⁷H.H. Bruun, *Hot-wire Anemometry – Principles and Signal Analysis*, (Oxford University Press, Oxford, 1995).
- ⁸H. Eckelmann, *Einführung in die Strömungsmesstechnik*, (Teubner Studienbuecher, Stuttgart, 1997).
- ⁹Due to the aspect ratio and the desired length wires would become thinner than $1\mu m$, which is too fragile for flows of several m/s .
- ¹⁰B. Castaing, B. Chabaud, F. Chilla, B. Hebral, A. Naert and J. Peinke, *J. Phys. III France*, **4**, 671 (1994).
- ¹¹O. Chanal, B. Baguenard, O. Bethoux and B. Chabaud, *Rev. Sci. Instrum.* **68** 2422 (1997).
- ¹²G. Binning, C.F. Quate and Ch. Gerber, *Phys. Rev. Lett.* **56**, 930 (1986).
- ¹³H. Stöcker, *Taschenbuch der Physik*, (Verlag Harri Deutsch, Thun und Frankfurt am Main, 1994).
- ¹⁴J. Fraden, *AIP Handbook of Modern Sensors. Physics, Designs and Applications*, (Springer, New York, NY, Berlin, Heidelberg, 1993).
- ¹⁵E.F. Schubert, *Light-Emitting Diodes*, (Cambridge Univ. Press, Cambridge, 2003), p.24.2.
- ¹⁶Further details of this experimental setup and typical results of local isotropic turbulence can be found in Renner.¹⁷
- ¹⁷C. Renner, J. Peinke and R. Friedrich, *J. Fluid Mech.* **433**, 383 (2001).
- ¹⁸J. Davoudi and M.R.R. Tabar, *Phys. Rev. E* **61**, 6563 (2000).
- ¹⁹U. Frisch, *Turbulence*, (Cambridge University Press, Cambridge, 1995).
- ²⁰J.O. Hinze, *Turbulence*, (McGraw-Hill, 1975).
- ²¹Note that the geometry of the cantilever chips may drastically affects the form of the pdfs. Using cantilever chips which are not flow optimized, like those for atomic force microscopy where the cantilever is at the side of a large rectangular base, the pdfs of the LCA measurement exhibit perturbed shapes.
- ²²R. Benzi, S. Ciliberto, R. Tripicciono, C. Baudet & S. Succi, *Phys. Rev. E* **48**, 29 (1993).
- ²³Arneodo A. et al., *Europhys. Lett* **34**, 411 (1996).
- ²⁴J. Peinke, B. Castaing, B. Chabaud, F. Chilla, B. Hebral and A. Naert, *Fractals in the Natural and Applied Sciences*, **A-41**, 295 (1993).
- ²⁵J. Mathieu, J. Scott, *An Introduction to Turbulent Flow*, (Cambridge University Press, Cambridge, 2000), p. 294.
- ²⁶J. Piquet, *Turbulent Flows - Models and Physics*, (Springer, Berlin, 2001), p. 185.